β-detected NMR of $^8Li^+$ in Bi, Sb, and the topological insulator $Bi_{0.9}Sb_{0.1}$

W. A. MacFarlane,[1] C. B. L. Tschense,[1,2] T. Buck,[3] K. H. Chow,[4] D. L. Cortie,[1,3,5] A. N. Hariwal,[6] R. F. Kiefl,[3] D. Koumoulis,[7] C. D. P. Levy,[8] I. McKenzie,[8,9] F. H. McGee,[3] G. D. Morris,[8] M. R. Pearson,[8] Q. Song,[3] D. Wang,[3] Y. S. Hor,[10] and R. J. Cava[11]

[1]*Department of Chemistry, University of British Columbia, Vancouver, BC, Canada V6T 1Z1*
[2]*Department of Inorganic Chemistry, University of Bayreuth, Bayreuth D-95440, Germany*
[3]*Department of Physics and Astronomy, University of British Columbia, Vancouver, Canada V6T 1Z1*
[4]*Department of Physics, University of Alberta, Edmonton, AB, Canada T6G 2E1*
[5]*Quantum Matter Institute, University of British Columbia, Vancouver, Canada V6T 1Z1*
[6]*Department of Physics and Astrophysics, University of Delhi, Delhi-110007, India*
[7]*Department of Chemistry and Biochemistry, University of California, Los Angeles, California 90095, USA*
[8]*TRIUMF, Vancouver, Canada V6T 2A3*
[9]*Department of Chemistry, Simon Fraser University, Burnaby, BC, Canada V5A 1S6*
[10]*Department of Physics, Missouri University of Science and Technology, Rolla, Missouri 65409, USA*
[11]*Department of Chemistry, Princeton University, New Jersey 08544, USA*

(Received 19 October 2014; revised manuscript received 22 November 2014; published 10 December 2014)

We report the NMR Knight shift and spin-lattice relaxation of $^8Li^+$ implanted ~100 nm into single crystals of semimetallic Sb, Bi, and topologically insulating $Bi_{0.9}Sb_{0.1}$. We find small negative shifts (of order 100 ppm) in all three. In the insulator, the shift is nearly temperature independent, while in Bi and Sb it becomes more negative at low temperature without following the bulk susceptibility, suggesting two distinct temperature dependent contributions, possibly from the orbital and spin response. However, a simple model is unable to account for the observed shift. The spin-lattice relaxation differs in both scale and temperature dependence in all three. It is Korringa-like in Bi and remarkably is fastest in the insulating alloy and slowest in Sb with the highest bulk carrier density. These surprising results call for detailed calculations, but phenomenologically demonstrate that β-detected NMR of implanted $^8Li^+$ is sensitive to the magnetic response of low-density carriers. The prospects for depth-resolved studies of conventional and topological surface states at lower implantation energies are good.

DOI: 10.1103/PhysRevB.90.214422 PACS number(s): 75.20.En

I. INTRODUCTION

Like conventional nuclear magnetic resonance, NMR detected by radioactive β decay provides a sensitive local probe of the electronic properties of solids. In particular, low-energy ion beams of the hyperpolarized β NMR isotope ^{8}Li, can be used to measure *depth-resolved* NMR in thin films and crystals [1–3], where conventional NMR is practically impossible due to the intrinsically small signal. In particular, we have shown that implanted $^8Li^+$ is a powerful probe of the metallic state [4–8]. We plan to use it to study the metallic topological surface state (TSS) of three-dimensional (3D) topological insulators (TIs) [9–12]; however, this necessitates a clear understanding of the signals in the bulk to clearly distinguish the TSS.

Here, we focus on the TI $Bi_{0.9}Sb_{0.1}$ [13], a small-gap semiconductor substitutional alloy of the elemental semimetals Bi and Sb. Although the bulk properties of these materials have been studied extensively, from a NMR viewpoint, they are not well known. For example, their magnetic properties are largely determined by valence electron orbital diamagnetism. The Pauli spin response, that is often preferentially sensed by the NMR Knight shift in metals, appears to play a minor role. Moreover, the spin response cannot be considered independent of the orbital response due to spin-orbit coupling that is particularly strong for bismuth. We thus include a brief introductory review in Sec. IV.

In this paper, we present $^8Li^+$ β NMR results on the elemental semimetals Bi and Sb and the TI alloy $Bi_{0.9}Sb_{0.1}$. We find (1) small negative shifts in all three, with a temperature-independent shift *only* for the insulating phase, and (2) temperature-dependent spin-lattice relaxation, that is Korringa-like *only* in Bi and remarkably is *fastest* in the TI. Thus, we establish that $^8Li^+$ β NMR is sensitive to low carrier density metals, indicating the prospects for sensitivity to the TSS are good, and define the bulk behavior that will constitute the background in measurements at much lower implantation energy to study the TSS. Although our main motivation is the TSS, these results are interesting in their own right, and we discuss them in the context of the NMR and μSR in semimetals and narrow-gap semiconductors.

II. EXPERIMENT

β NMR is based on the parity-violating weak interaction that causes the angular distribution of the emitted β radiation to be correlated with the spin direction of the decaying nucleus at the instant of decay. The technique was pioneered shortly after the discovery of parity violation [14], but unlike μSR [15,16] it has not been widely used as a probe of condensed matter [17]. Its sensitivity is similar to that of the μ^+, but specific properties of the nucleus distinguish it in a number of important respects, notably the lifetime of the β NMR probe is generally much longer.

β NMR measurements were made by implanting spin-polarized $^8Li^+$ at kinetic energy ~20 keV into the single-crystal samples. The ^{8}Li, nucleus has spin $I = 2$, gyromagnetic ratio $\gamma = 6.3015$ MHz/T, and electric quadrupole moment $Q = +31.4$ mb. The spin is polarized by in-flight optical pumping to polarization ~70% [18]. Resonances were

acquired in a dedicated spectrometer [19] with continuous wave (CW) transverse radiofrequency (rf) magnetic field with frequency stepped slowly relative to the ^{8}Li, lifetime $\tau = 1.21$ s through a range around the probe's Larmor frequency in the homogeneous static field B_0 of 6.55 or 2.2 T applied perpendicular to the surface of the crystals (parallel to the trigonal c axis). The beam intensity was on the order of 10^6 ions per second into a beamspot ~2 mm diameter centered on the sample.

As a frequency calibration, the resonance in a single crystal of MgO [20] was measured at 300 K with the superconducting solenoid in persistence mode. Each resonance spectrum takes ~ 60 min to acquire. The relative shift of the resonance from its position in MgO was then calculated as

$$K_{\rm raw} = \frac{\nu - \nu_{\rm MgO}}{\nu_{\rm MgO}}. \quad (1)$$

In metals, the shift is typically dominated by the Knight shift, proportional to the Pauli spin susceptibility, that has been very important in the understanding of the degenerate metallic state [21].

For the measurements, the bismuth crystal was freshly cleaved in air at ~77 K, while the others do not easily cleave, and were used with the native crystal surfaces. For Sb, we compare two crystals. The $Bi_{0.9}Sb_{0.1}$ alloy was a flat platelet crystal 3.4×3.9×0.4 mm prepared as in Ref. [13]. The crystals were afixed to an 8×10 mm Al_2O_3 substrate with Ag paint which was then clamped to a UHV coldfinger liquid-helium cryostat.

Ion implantation at keV energies into solids is a statistical process that results in a distribution of implantation depths, the implantation profile. Computer simulation of ion stopping is a reliable means of simulating the implantation profile. Using the SRIM2013 package [22], we calculated the ^{8}Li$^+$ profiles for the relevant energies for this experiment. The results, shown in Fig. 1, indicate that the mean implantation depth is about 100 nm. These calculations, based on the binary collision approximation, take no account of the crystal structure of the host and thus do not include implantation channeling [23]. When it occurs, channeling results in a long tail of the implantation profile deeper into the crystal, corresponding to the channeled fraction. Based on the crystal structure (see Sec. IV B), we do not expect the trigonal axis of $Bi_{1-x}Sb_x$ is a channeling direction.

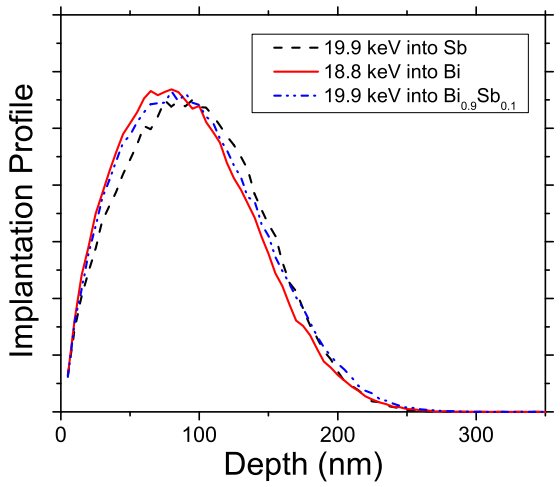

FIG. 1. (Color online) Calculated implantation profiles for ^{8}Li$^+$ in Bi, Sb, and $Bi_{0.9}Sb_{0.1}$ from SRIM2013 [22] at the energies used in the experiment. The mean range is about 100 nm and a negligible fraction of the ^{8}Li$^+$ stop in the top 10 nm, where one may expect the properties to be modified by surface states.

The NMR shift measures the average local field at the nucleus in the surrounding material. One contribution to this field is demagnetization, which combined with the Lorentz sphere generates a relative shift of the resonance that can be corrected by adding [24]

$$K_d = 4\pi\left(N - \tfrac{1}{3}\right)\chi, \quad (2)$$

where N is the shape-dependent demagnetization factor. In the limit of a thin film, $N = 1$, but for the samples here, we estimate $N \approx 0.8$. To evaluate K_d as a function of temperature requires the (cgs volume) susceptibility χ. We use values from the literature [25–28] fit to a phenomenological form. The resulting corrections are shown in the following section. As χ is negative (diamagnetic), the demagnetizing field shifts the resonance to *higher* frequency, and the correction K_d is negative. The corrected Knight shift is then defined as

$$K_c = K_{\rm raw} + K_d \quad (3)$$

and represents the shift due to hyperfine fields at the ^{8}Li$^+$ probe. For light NMR nuclei such as ^{8}Li, the hyperfine shift is small (~100 ppm) due simply to the small hyperfine coupling. Therefore, in contrast to transition-metal NMR where the hyperfine shift is often in the range of %, here K_d is an important and relatively large correction (see Sec. 5.5 of Ref. [21]).

Spin-lattice relaxation data are collected without any rf magnetic field by implanting a pulse of beam and monitoring the spin polarization as a function of time both during and after the pulse, repeating the cycle to obtain the required statistics, alternating the polarization direction by controlling the sense of the polarizing laser light. The resulting data are fit with a spin-relaxation function convoluted with the beam pulse to extract the relaxation rate.

III. RESULTS

In bismuth, the spectrum consists of a set of well-resolved small satellite lines near the Larmor frequency $\nu_0 = \gamma B_0$ (see Fig. 2). With the rhombohedral crystal symmetry, we expect finite electric field gradients (EFGs) at all sites in the structure. The EFG, characteristic of the ^{8}Li$^+$ site, couples to its nuclear electric quadrupole moment, splitting the NMR into a set of satellites corresponding to the (primary) $|\Delta m| = 1$ transitions among the $2I + 1 = 5$ magnetic sublevels (indexed by m). For a particular site, we thus expect a pattern of four satellites symmetrically distributed about the resonance position.

In high field ($\nu_Q \ll \nu_0$), the primary satellite positions are given by the first-order formula [29]

$$\nu_{m\leftrightarrow m-1}|_{m=-1\ldots2} = (1+K)\nu_0 - \nu_Q\left(m - \tfrac{1}{2}\right)f, \quad (4)$$

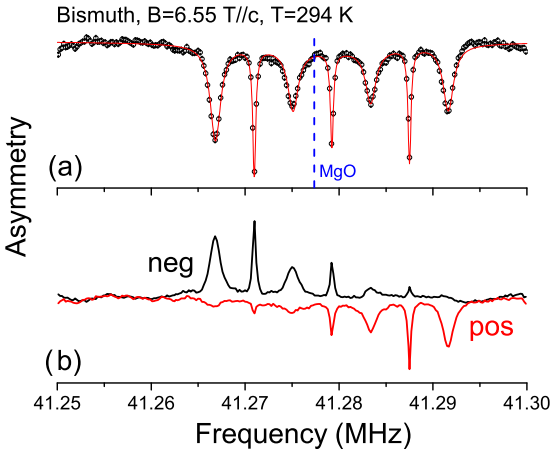

FIG. 2. (Color online) The resonance spectrum of $^8Li^+$ in bismuth, exhibiting four broader quadrupolar satellites and three sharper multiquantum resonances. (a) The combined asymmetry spectrum (combining the two helicities) together with a fit described in the text. The vertical dashed line marks the position of the resonance of $^8Li^+$ in MgO at 300 K in this field, chosen as the reference of zero shift. (b) The spectra for the two laser helicities, the asymmetry of the spectrum about its center confirms the quadrupolar nature of the splitting.

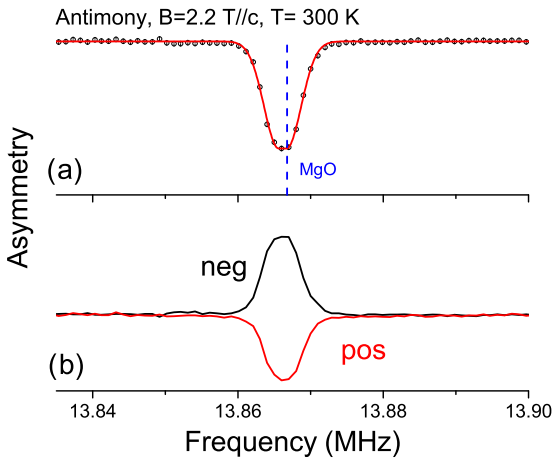

FIG. 3. (Color online) (a) The helicity-combined and (b) helicity-resolved spectra in antimony at 300 K. The curve in (a) is the fit described in the text. The slight asymmetry in (b) may reflect unresolved quadrupolar splittings.

where $\nu_Q = e^2qQ/4h$, e is the electronic charge, and f is a function of angle between the coordinate systems defined by the applied field and the EFG. For an axisymmetric EFG, this depends on only θ, the angle between the applied magnetic field and the principal symmetry axis of the EFG tensor eq, and

$$f = \tfrac{1}{2}[3\cos^2(\theta) - 1]. \quad (5)$$

The ideal spectrum then consists of a pair of satellites on each side of the Larmor frequency with the outer satellite splitting $3\times$ that of the inner satellite. A lower symmetry site will likely result in further splittings due to sites which are not equivalent under the applied field. The satellite amplitudes depend on the detailed magnetic sublevel populations of the polarized beam, but generally the $m = \pm 2$ is highly populated making the *outer* satellites more intense. The quadrupolar nature of the splitting is clearly evident in the antisymmetry of the helicity-resolved spectra about the center in Fig. 2(b), where the two curves correspond to polarization in the opposite sense. For example, the outermost satellites correspond to the $m = \pm 2 \leftrightarrow \pm 1$ transitions. For completely polarized ^{8}Li, the spectrum would consist of only this lower (upper) satellite for negative (positive) helicity. For the highly polarized beam, these outer satellites are still dominant in the corresponding helicity spectra, but the inner satellites are also visible.

The combined spectrum contains the expected quartet of satellites together with a triplet of much narrower interleaved resonances. The satellite pairs forming the quartet have similar widths and their splittings (8.3 and 24.94 kHz) from the center of the pattern satisfy the expected ratio of 3 from Eq. (4). The narrow lines are consistent with multiquantum resonances [30] based on their positions midway between the primary satellites, their narrowness from the absence of first-order quadrupolar broadening [31], and their strong dependence on rf field (not shown). In fact, the resonance pattern is so well resolved that we have used it to determine the detailed level populations of the ^{8}Li, [30]. The splitting is also found to be independent of B_0 in the range 2.2 to 6.55 T, consistent with a quadrupolar origin. We fit the spectrum to a sum of Lorentzians with splittings determined by a single parameter ν_Q as shown in the figure. From this we accurately determine the center of the overall pattern and its displacement relative to the reference measurement in MgO.

The spectrum in antimony (Fig. 3) is remarkably different with no quadrupolar splitting and instead a single resonance somewhat broader than the Bi satellites. This is unexpected since Sb has the same crystal structure and must have nonzero EFG at the $^8Li^+$ site. With a smaller lattice constant, one might even expect a higher EFG and larger splittings in Sb. The spectrum was so different, in fact, that we confirmed it on a second Sb crystal, from a different source, with consistent results. The helicity-resolved spectra in Fig. 3(b) show a slight antisymmetry about the center, suggesting some unresolved quadrupole splittings. Above 150 K, the spectrum is noticeably flat topped, so it was fit with a flat-topped Gaussian, i.e., a square shape with Gaussian wings. Below 150 K, a simple Gaussian was adequate. As is expected in the absence of resolved quadrupolar splittings, the resonance is much larger in amplitude than the satellites in Bi. The resonance position and its displacement from MgO were determined from these fits.

Again in $Bi_{0.9}Sb_{0.1}$, only a single resonance is observed with no evidence of quadrupolar splittings. The resonance was best fit with a pseudo-Voigt function

$$f(\nu) = \eta\mathcal{L}(\nu) + (1-\eta)\mathcal{G}(\nu), \quad (6)$$

where $\mathcal{L}$ and $\mathcal{G}$ are a Lorentzian and Gaussian of the same width, and η is a parameter varying from 0 to 1 as f changes from a pure Gaussian to a pure Lorentzian. This line shape likely results from power broadening of a broad Gaussian. An example is shown in Fig. 4. Although the resonance is large, and the statistical error bars small, *systematic* baseline drifts make the extracted resonance position more scattered in this case.

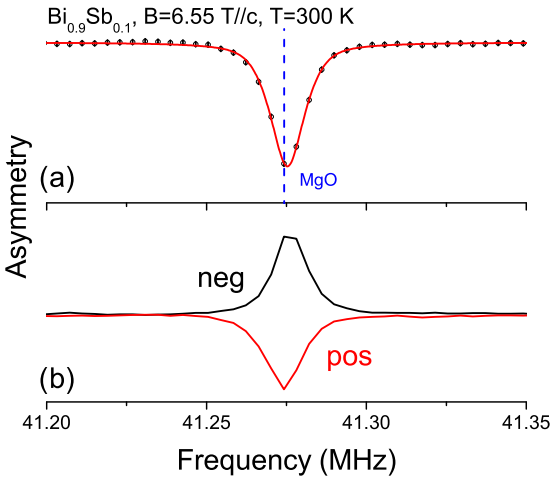

FIG. 4. (Color online) The resonance of $^8Li^+$ in the $Bi_{0.9}Sb_{0.1}$ crystal, showing no evidence of resolved quadrupolar splitting. (a) The combined asymmetry together with the fit described in the text. (b) The helicity-resolved spectra show only a slight asymmetry.

The raw shifts for each sample are plotted as a function of temperature in Fig. 5(a) and the demagnetization corrected values in Fig. 5(b), using the corrections shown in Fig. 5(c). Although it is more scattered than the others, the shift in $Bi_{0.9}Sb_{0.1}$ shows little or no systematic temperature dependence, while the shifts in both Bi and Sb move downward as the temperature is reduced. As the demagnetization correction K_d is larger at low temperature, the decrease in the raw shift is enhanced in K_c. The sample furthest from the thin plate limit assumed for the demagnetization is the Sb crystal. Measurement of the second Sb crystal at 300 K shows a small difference in shift, some of which is due to a difference in the sample shape. Finally, in Bi, the crystal was measured at two fields (6.55 and 2.2 T) at 300 K, confirming that the shift is magnetic, i.e., the relative shift is field independent.

The resonance linewidths from the fits (expressed as HWHM) are shown in Fig. 5(d). There is a clear hierarchy: the satellites in Bi are narrowest and the resonance in $Bi_{0.9}Sb_{0.1}$ is widest. The widths are only weakly temperature dependent, apart from a narrowing in Sb above 300 K, there is a low-temperature broadening in Bi below 50 K.

For each sample, spin-lattice-relaxation data were collected using a 4 s long beam pulse followed by a counting period typically 12 s. The results near room temperature are shown in Fig. 6. It is immediately obvious that, at this temperature, the relaxation is slowest in Sb and fastest in the alloy. The data were fit to a single exponential relaxation convoluted with the square beam pulse, i.e., the polarization of an ^8Li, spin at a time t after its implantation follows $\exp(-\lambda t)$, where $\lambda = 1/T_1$ is the relaxation rate. The single exponential fit works well except during the first second of the beam pulse, due to a small fast relaxing background signal. We thus exclude these early times from the fitting. The relaxation in both Bi and Sb at low temperature is quite slow, near the limit of reliable measurement determined by the probe's radioactive lifetime τ. The resulting values of λ are plotted as a function of temperature in Fig. 7.

There is also evidently a hierarchy of relaxation rates, with the fastest relaxation corresponding to *insulating* $Bi_{0.9}Sb_{0.1}$.

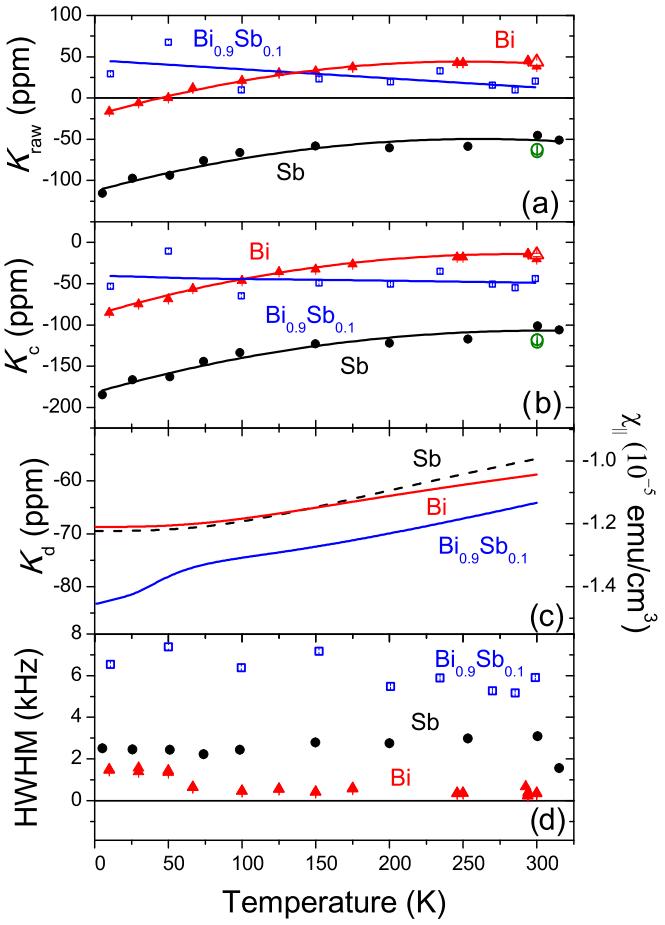

FIG. 5. (Color online) As a function of temperature, from fits to the resonance spectra for $^8Li^+$ in Bi (red triangles), Sb (black circles), and $Bi_{0.9}Sb_{0.1}$ (blue squares): (a) the raw shift from MgO; (b) the demagnetization corrected Knight shift; (c) the demagnetization correction defined by Eq. (2), using literature values of the volume susceptibility $\chi_\parallel$ (right scale); and (d) the linewidths (HWHM). For bismuth this is the single quantum satellite width. The open green circles are measurements made on a second Sb sample. The field is 6.55 T, except Sb and the open triangles (Bi) where it is 2.2 T.

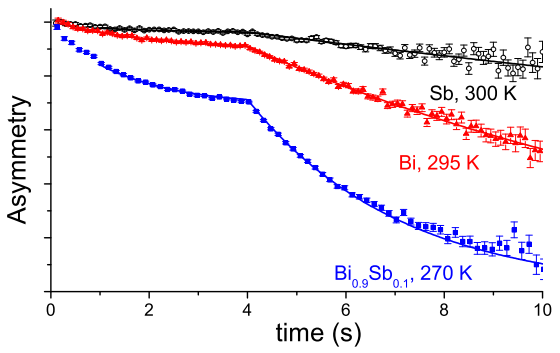

FIG. 6. (Color online) The time dependence of the asymmetry during and after a 4 s beam pulse at 6.55 T for each sample near room temperature. Single exponential fits excluding the first second are also shown as the solid curves.

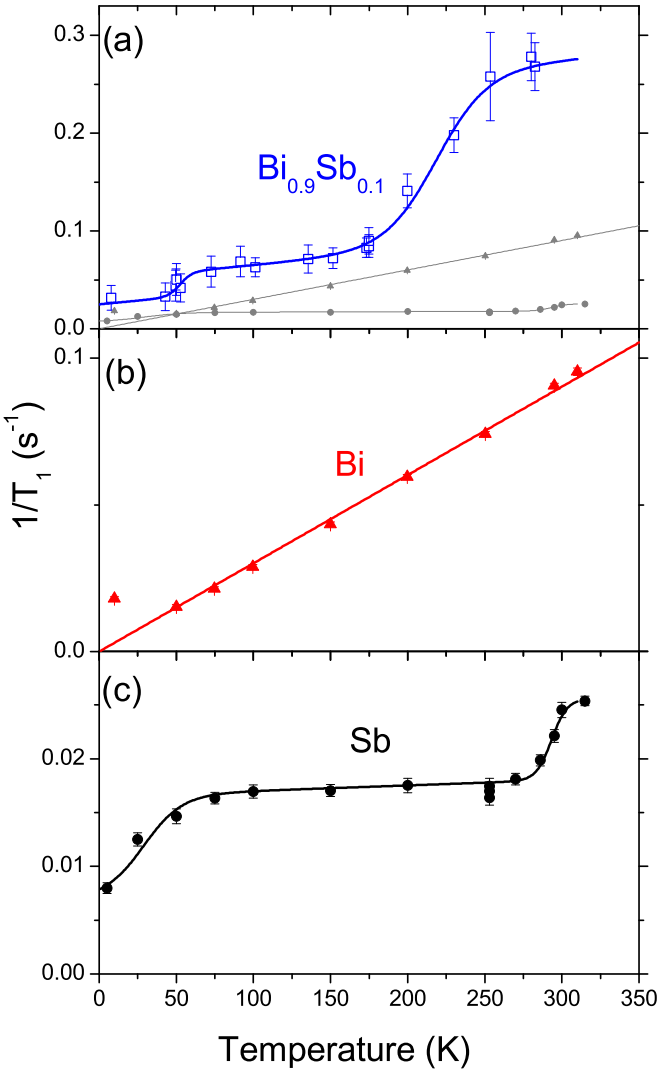

FIG. 7. (Color online) The spin-lattice-relaxation rates $(1/T_1)$ for $^8Li^+$ in (a) $Bi_{0.9}Sb_{0.1}$, (b) Bi, and (c) Sb in 6.55 T field as a function of temperature. The data for Bi and Sb are replotted in grayscale in panel (a) to show the rates on the same scale. The curves are guides to the eye.

The temperature dependence in Bi is simply linear as might be expected in a metal. The lowest temperature point deviates from the line, but the relaxation here is very slow, near the limit of measurement. Fitting all but the lowest T yields a slope $3.02(3)\times10^{-4}$ s^{-1} K^{-1}. The temperature dependence of neither antimony nor $Bi_{0.9}Sb_{0.1}$ is similar. In Sb there appears to be a steplike feature near room temperature and a decrease below 50 K, while in $Bi_{0.9}Sb_{0.1}$ there is a step near 200 K and another smaller one around 50 K. The hierarchy in λ is seen clearly when plotted on the same scale as in Fig. 7(a).

IV. DISCUSSION

A. Introduction

With the basic results presented above, we have a microscopic probe of the electronic state of $Bi_{1-x}Sb_x$. As context for the following discussion, here we summarize some of the properties of pure Bi and Sb and their alloys, particularly as seen by hyperfine coupled spin probes.

The electronic properties of the continuous solid solution series $Bi_{1-x}Sb_x$ have been studied extensively. The pure end members are well known semimetals, while at intermediate concentrations, between about 8% and 22% Sb, there is a small but finite gap at the Fermi level, making it a narrow-gap semiconductor. At its maximum, the gap is only ~20 meV [32]. Alloys in this composition range were first theoretically proposed [33], and subsequently shown experimentally [13], to be three-dimensional topological insulators with an insulating state characterized by a nontrivial topological invariant and a protected metallic surface state, but they have long been studied for potential thermoelectric applications [32,34], as well as for a fundamental understanding of the metallic state, notably including the discovery of quantum oscillations [35].

1. Electronic structure

Here, we summarize the electronic structure of $Bi_{1-x}Sb_x$, beginning with bismuth. This will be important in discussing the results in comparison with the familiar case of NMR in metals.

Quantum oscillations, persisting to relatively high temperature, allowed the small Fermi surface of Bi to be mapped out and compared in detail to band-theory calculations, and a great deal is understood about its electronic structure as a result [36,37]. Both the valence and conduction bands are derived from the valence p atomic orbitals, while the s band is substantially lower in energy. The valence band cuts through the Fermi level at the T point in the Brillouin zone, giving rise to two hole pockets. Here, there is a substantial gap up to the conduction band (~0.75 eV), so no appreciable cross-gap excitations occur. The conduction band also crosses E_F at the L point, giving rise to six electron pockets [37,38]. Here, in contrast, the energy gap to the filled valence band below E_G is very small (~15 meV), and this has important consequences for the electronic, and particularly the magnetic, properties (see below). The dispersion is highly curved in the vicinity of E_F, giving rise to small effective masses m^*, which are also important for the magnetic response. The Fermi surfaces are small disconnected pockets corresponding to small electron and hole densities on the order of 3×10^{17}/cm^3. This form of the Fermi surface results from a delicate balance between the slight rhombohedral lattice distortion and the effects of spin-orbit coupling (λ_{SO}). The lattice is centrosymmetric, so the bands remain twofold (Kramers) degenerate, but the degeneracy is not pure spin due to λ_{SO}. Detailed band-structure calculations are available [39–41] as well as an optimized tight-binding parametrization [42]. The Fermi energies are also very small, ~10 meV for the holes and ~25 meV for the electrons [36]. The density of states $\rho(\epsilon = E - E_F)$ for this band structure exhibits a pronounced narrow *minimum* at E_F, in a sense the inverse of the sharp d band peak at E_F that is important in determining the magnetic properties of transition metals such as Pd [4]. Within ±150 meV of E_F, $\rho(\epsilon)$ is approximately described by

$$\rho(\epsilon) \approx a + b\epsilon^2. \quad (7)$$

A magnetic field modifies the electronic spectrum by Landau quantization. Due to the small m^* in bismuth, the level spacing is quite large, and one can obtain the quantum limit, where only the lowest Landau level is occupied, at accessible magnetic fields [43]. Landau spectra in Bi as a function of field have recently been studied quantitatively [44].

A convenient simplification of the electronic structure focuses on the two bands near E_F at the L point [38], neglecting the hole pockets. Here, the spectrum was shown to be analogous to the relativistic Dirac equation [44–46]. Dirac-type electrons have distinctive features, in particular, in their response to a magnetic field. Unlike the free-electron Landau spectrum, the level spacing is not uniform, and the lowest level is pinned to the band edge [47].

The electronic structure of antimony is closely related to bismuth but not as extensively studied. For Sb, the shape of the electron pockets is similar, but the hole pockets become a complex multiply connected sheet, the Lin-Falicov surface [48]. The Fermi surface is larger, corresponding to the 100× higher carrier density. The gap at L is also larger (∼110 meV [49]), making the effects of the filled valence band below the electron pockets less important. E_F is larger: about ∼100 meV for both electrons and holes, and λ_{SO} is substantially smaller.

The alloy is also well studied [50], but disorder hinders as complete a theoretical description, complicates the preparation of homogeneous samples, and limits the electronic mean-free path, suppressing quantum oscillations. The lattice parameters vary smoothly with x but slightly nonlinearly [51]. The band structure is generally discussed in the coherent potential approximation that neglects completely the effects of disorder, just treating the alloy as a periodic virtual material. The evolution of this mean-field electronic structure with x has been studied experimentally [32]. Band energies near E_F vary on scales of 100 meV, interpolating between Bi and Sb. Crucial to the nontrivial topological insulator [52] is the inversion of the valence and conduction bands (having different symmetries) that occurs in the semimetallic phase at $x \sim 0.04$ [53]. For the specific composition $Bi_{0.9}Sb_{0.1}$, the gap at the L point E_G, now properly the semiconductor band gap, is about 10 meV at low temperature [32].

In addition to widespread interest in topological insulators, the physics of semimetals is currently enjoying renewed interest [54,55] since some high-T_c cuprate and Fe-pnictide/chalcogenide superconductors exhibit small semimetallic Fermi surface pockets. However, here, in bismuth, in contrast to the cuprates, conventional electron correlations should be *negligible* as the carriers are light, low density, and their dielectric screening is strong [56], though some unusual electron interactions have been found [57]. Quantum phenomena in Bi have also been the subject of considerable recent interest [43,44,58,59]. Extensive work has also been done studying the nontopological surface states of Bi [60]. Due to the small Fermi wave vector, finite-size effects are also prevalent and widely studied [61,62].

2. *Magnetic properties*

Key to the interpretation of our results are the magnetic properties of $Bi_{1-x}Sb_x$ resulting from the electronic structure summarized above. At all compositions, it is strongly *diamagnetic*, and the rhombohedral structure renders χ anisotropic. The relevant component is $\chi_\parallel$, the response along the trigonal axis. χ is also temperature dependent, with $\chi_\parallel(T)$ becoming more negative, by about 20%, from 300 to 4 K [see Fig. 5(c)].

Generally, χ is composed of several contributions, and the NMR shift K may be differently sensitive to each of them. In typical metals, K is primarily due to the (Pauli) spin susceptibility of the conduction band $\chi_{\rm Pauli}$, which is usually independent of T. However, in cases where χ depends on T, such as Pt and Pd, the temperature dependence of the shift can be correlated to a temperature-dependent contribution to χ to determine the hyperfine coupling [4,5,63]. As a starting point, following Ref. [64] and others, we consider χ composed of several terms

$$\chi = \chi_{\rm core} + \chi_{\rm FS}(T) + \chi_{\rm VB}(T), \tag{8}$$

where $\chi_{\rm core}$ is the (Larmor/Langevin) diamagnetic susceptibility of the closed-shell ion cores Bi^{5+}/Sb^{5+}. It is isotropic, independent of T, and estimated to be about ∼10% of the total χ at 4 K. The carriers (electrons and holes at E_F) contribute $\chi_{\rm FS}$ which is composed of the paramagnetic spin part and the orbital (Landau) diamagnetism

$$\chi_{\rm FS} = \chi_{\rm Pauli} + \chi_{\rm Landau}. \tag{9}$$

For a free-electron gas, we have the well-known relation $\chi_{\rm Landau} = -\chi_{\rm Pauli}/3$. However, in the semimetals, we must use the Peierls generalization of $\chi_{\rm Landau}$ which is magnified by the factor $(m/m^*)^2$, where m^* is the band effective mass. One might think this term could then account for the remaining diamagnetism, but this is not the case because the paramagnetic spin response is also amplified by a similarly large factor $g_{\rm eff}^2$ [65]. In fact, the band and cyclotron masses are similar [66], so the net $\chi_{\rm FS}$ is *positive* as for the free-electron gas.

$\chi_{\rm FS}$ can be further decomposed into contributions from the (L point) electrons and the (T point) holes. For $\chi_\parallel$ from the L electrons in pure Bi, the two terms in $\chi_{\rm FS}$ almost completely cancel, while the cancellation is substantially less for the holes, and the hole contribution is the dominant part of $(\chi_{\rm FS})_\parallel$. In addition, unlike the free-electron gas, one cannot treat the density of states $\rho(\epsilon)$ as constant on the scale of kT, so $\chi_{\rm FS}$ is temperature dependent. For the insulator, the band gap (at L) is small, so carriers are thermally excited at 300 K, and $\chi_{\rm FS}$ is nonzero, but it should disappear as $T \to 0$. Indirect estimation of $\chi_{\rm FS}$ predicts that it accounts at most 1% of the total [28]. Estimates based on the Sommerfeld coefficient of the specific heat (for either Bi or Sb) are even less (∼0.1%) [21]. Thus, the bulk χ yields no information on $\chi_{\rm Pauli}(T)$. $\chi_{\rm Pauli}$ is a quantity of fundamental interest, providing an important test of models of the electronic structure at the Fermi level. It would thus be very useful to measure it. NMR shifts are often the only way to accomplish this, but this has not been possible in Bi or Sb (see the following section).

In fact, the decomposition of χ in Eq. (8) is not so clear-cut. The orbital response to the magnetic field has interband terms that involve states both at E_F and below. Moreover, the very strong λ_{SO} implies that spin is not a good quantum number for electrons at E_F, so a conventional Pauli term is not justified. Kramers degeneracy is preserved in the bulk, so one can define

an effective spin, but this mixes in the orbital response, and the two cannot be treated separately. Fukuyama and Kubo [67] first showed how to calculate χ with full inclusion of the spin-orbit coupling, using the Dirac-type spectrum in Bi [45]. The result can also be expressed compactly using a Green's function approach [68], but it does not break up into a simple sum of terms as above. Such a decomposition is, however, natural for hyperfine probes that are coupled differently to the orbital and spin degrees of freedom. For the moment, we adopt the view that a decomposition of the form Eq. (8) can at least be made approximately, but we return to this point in the following.

The main source of the diamagnetism of $Bi_{1-x}Sb_x$ is, in fact, the third term in Eq. (8) χ_{VB}, the orbital contribution (via the interband effect of the field) of the filled valence bands below the Fermi level response [69,70]. Normally χ_{VB} would be small, but here, due to the very small gap, it is large and temperature dependent, due to $E_G(T)$ [71]. χ_{VB} scales with $1/E_G$, and, for Bi, it has been calculated in detail for a simplified electronic structure [64,67,70] as well as for dilute $Bi_{1-x}Sb_x$ alloys [72]. The effect of composition x was studied carefully experimentally [28] and was a crucial test of this theory.

No comparable calculation exists for antimony, likely due to the more complex band structure near E_F. Remarkably, Sb's diamagnetism is comparable to Bi despite the substantially larger Fermi surface and larger energy gap. The carrier term χ_{FS} is thought to be smaller, due to the reduced effective masses [28]; however, the Sommerfeld estimate is about 5× larger than Bi [21]. The largest term is again expected to be χ_{VB}. It would be interesting to apply modern strategies to calculate χ for Sb [73].

Unlike Pt metal, where a single term in χ, the d band χ_{Pauli}, is temperature dependent, we have two terms in Eq. (8) with distinct T dependencies, with one of them, $\chi_{VB}(T)$, predominantly determining the overall χ. On the other hand, the contact hyperfine interaction of the ^{8}Li, nucleus with the host band structure will provide a coupling to $\chi_{Pauli}(T)$ which, as above, is a negligible fraction of the bulk χ. One may then expect that $K(T)$ may be quite different than the bulk $\chi(T)$. However, one should consider whether the orbital χ_{VB} might have a substantial coupling to the ^{8}Li, nucleus. Often, in metals, such orbital shifts are small compared to the Knight shift, but this may not be the case here as will be discussed further in the following section.

3. *NMR, μSR and related probes*

The NMR of semimetals and narrow-gap semiconductors has some significant differences from the more familiar case of metals [74,75]. Here, one finds small values of the Fermi energy E_F and substantial structure in the electronic density of states $\rho(\epsilon)$, making the usual low-temperature expansion of the Fermi-Dirac distribution invalid for calculating such properties as the magnetic response. Consequent modifications to the Korringa relaxation have been treated theoretically [76–78]. While NMR in semimetals is at a much more primitive state than in metals, some phenomenology is available, for example, from semimetallic compounds [79], while an extensive literature on narrow-gap semiconductors exists, particularly the cubic Pb chalcogenides [80–83], where, as in Bi, the spin-orbit interaction plays an important role.

NMR in solid Bi and Sb has proven difficult due to very large quadrupolar splittings ($\nu_Q > 50$ MHz), and few results are available [21]. In Bi, there is a large negative shift at 4.2 K with significant anisotropy [84], but its temperature dependence has not been explored. The shift in Sb is even less certain [85], but the pure quadrupolar resonance (NQR) has been measured, finding Korringa behavior in the spin-lattice-relaxation rate $1/T_1$ [86,87] up to about 100 K, above which it increases supralinearly, though still the relaxation is magnetic [87]. $Bi_{1-x}Sb_x$ alloys, with random distributions of large quadrupolar splittings are even less amenable to study with available stable nucleus NMR, and no reports exist.

In contrast, the Knight shift of the implanted positive muon has been measured in detail in Bi [88,89], Sb [90–92], and $Bi_{1-x}Sb_x$ [89,93] by μSR (see the review by Cox [94]). The implanted spin-$\frac{1}{2}$ muon has no quadrupole moment, making it a pure magnetic probe; however, generally the Korringa relaxation is so slow on its time scale (2.2 μs) that it is nearly always unobservable [95]. Stroboscopic μSR, which allows accurate measurements of the typically small (∼100 ppm) muon Knight shifts in metals [15], was used to study the shift in Bi and dilute $Bi_{1-x}Sb_x$ alloys. For bismuth a relatively large negative K_μ is found, about −250 ppm at 4.2 K [89], with a large and unusual anisotropy at low temperature [88]. Both isotropic and anisotropic K_μ are found to scale with the bulk χ, with a scaling independent of x up to at least 0.37, but dependent on orientation [89,93].

In antimony, $K_\mu(T)$ is unrelated to the bulk $\chi(T)$ as the μ^+ traps an electron to form a paramagnetic muonium atom that is strongly coupled to the conduction band, behaving as a Kondo impurity [92]. A similar effect is seen for μ^+ in semimetallic graphite [96]. With its substantially lower ionization energy, we do not expect anything similar for the implanted $^8Li^+$.

Perturbed angular distribution (PAD) has also been used to study the Knight shift of heavy element substituents in bismuth [97,98]. They find a large negative shift for elements with an unfilled p shell, that disappears for closed-shell ^{211}Rn, and conclude that a diamagnetic orbital shift, rather than a negative hyperfine coupling to the carriers, predominates in bismuth in agreement with Ref. [99]. The absence of a negative shift for Rn has an uncertainty of ±2000 ppm, small compared to the other heavy element shifts, but an order of magnitude larger than our closed-shell $^8Li^+$ shift or K_μ. β NMR (using ^{8}Li, formed by polarized neutron activation) has been used previously to study Li/Bi mixtures, but this work was confined to the liquid state [100].

An important consideration for interpretation of our results is the origin of *negative* Knight shifts. Positive Knight shifts, due to contact hyperfine coupling to the Pauli spin susceptibility, are widely known in the NMR of metals. In d-band transition metals, core polarization can make the net coupling negative. In contrast, a coupling of nuclei to the diamagnetic orbital response of the free carriers is usually neglected as being much smaller than other contributions, e.g., in Pt [63]. Such a negative contribution, however, may be important here, where the diamagnetism is particularly strong [99,101–103].

The similarity of K_μ and χ in Bi and dilute $Bi_{1-x}Sb_x$ is a clear indication that the implanted muon senses the intrinsic magnetic response, specifically the predominant orbital term $\chi_{VB}(T)$ that is by far the largest contribution to χ. The obvious interpretation is that K_μ is an *orbital shift* in contrast to a Knight shift related to χ_{Pauli} as was suggested in Ref. [93]. As we have seen above, there is no reason to expect that χ_{Pauli} has the same T dependence as χ_{VB} since they are controlled by different quantities, χ_{VB} by the energy gap and χ_{Pauli} by $\rho(\epsilon)$ in the vicinity of the Fermi level. While the demagnetization field (which includes the long-range part of the orbital response) is accounted for in calculating K_μ [93], local orbital currents within the unit cell could well give rise to a field at the muon. Such currents would not be due to electronic bound states of the μ^+ (i.e., Mu levels), which appear to be unoccupied in Bi. Rather, they are due to circulating valence electron currents [102]. Moreover, if K_μ were due to $\chi_{Pauli}(T)$, one would expect it to be zero at low temperature in the semiconductor. It would be interesting to calculate, or at least estimate, whether such a large orbital shift is reasonable for the muon. Detailed calculations have been done for the simpler case of the ^{13}C shift in graphite [104], for example, *ab initio* [105,106] and other approaches [107] have also been developed for this problem, the challenge is to implement them for the case of an isolated charged point defect.

Having summarized the relevant literature, we now move on to discuss our results.

B. $^8Li^+$ spectra and site

Implanted $^8Li^+$ usually adopts a high-symmetry crystallographic site in the host. All three crystals possess the rhombohedral "arsenic" (A7) structure. Rather than the rhombohedral unit cell, one can consider a larger hexagonal unit cell with lattice parameters $a = 4.546, 4.522, 4.308$ and $c = 11.862, 11.810, 11.273$ Å in Bi, $Bi_{0.9}Sb_{0.1}$, and Sb, respectively [51]. In this cell, it is easier to see the layered structure composed of alternating bilayers of covalently bonded sheets. Each Bi/Sb is bonded to three nearest neighbors. Within this structure, there are two quasicubic interstitial sites with eight near neighbors, one is stretched (prolate, labeled P) along the trigonal axis, while the other is compressed (oblate, labeled O) along this axis [108]. Each of these sites (shown in Fig. 8 has six equivalent neighbors and two that are slightly farther (P) or slightly closer (O). Both these sites lie on the threefold symmetry axis and hence the EFG must be axial. The quadrupolar splitting of $^8Li^+$ in Bi is consistent with either of these axisymmetric sites, but the $B_0 \parallel c$ spectrum is not sufficient to guarantee an axial EFG.

The spectra in Sb and $Bi_{0.9}Sb_{0.1}$, however, show no resolved quadrupolar splitting. Their helicity-resolved spectra [Figs. 3(b) and 4(b)] do show slight asymmetry in the opposite helicity channels suggesting unresolved quadrupole splittings. Crystalline imperfections (dislocations, stacking faults, vacancies, impurities, etc.) result in a random distribution of EFGs at the $^8Li^+$ site, and this can yield a broad featureless spectrum. The $Bi_{0.9}Sb_{0.1}$ crystal is much closer to pure Bi in terms of the lattice constants, although here there is another source of randomness in the EFG, namely, the random Bi/Sb site occupation. Figure 9 shows the spectra at room temperature in

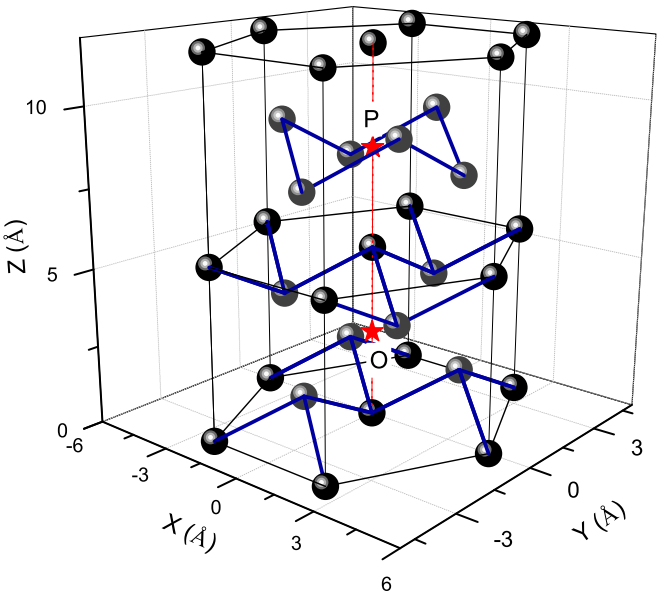

FIG. 8. (Color online) The hexagonal unit cell of the A7 crystal structure. The spheres represent Bi/Sb and the heavy lines represent the layered bonding network with each Bi/Sb bonded to its three nearest neighbors. Two high-symmetry interstitial sites are identified by the stars. They are at the center of a quasicube of surrounding atoms, but the cube is distorted by stretching (P) or compressing (O) along the trigonal axis (red line), along which the magnetic field is applied in the experiment.

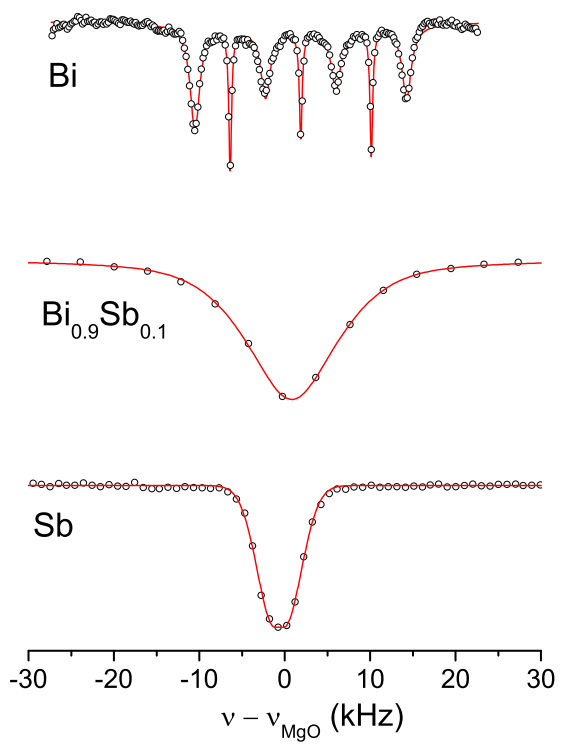

FIG. 9. (Color online) The spectra at room temperature (from Figs. 2–4) shown on the same horizontal scale as shift from MgO in kHz. The vertical scales differ for each. The curves are the fits described in the text.

the three samples on the same horizontal scale. The line shapes in $Bi_{0.9}Sb_{0.1}$ are qualitatively compatible with unresolved quadrupolar splittings of a similar magnitude to the resolved splitting in Bi. This is consistent with exceptional crystallinity of the Bi, which is reflected in the width of the satellite lines. In Sb, the scale of the quadrupolar splitting appears to be smaller by at least a factor of 2.

The implanted $^8Li^+$ may stop at a metastable site, where at low temperature it can be trapped, while at higher temperature it may make a thermally activated site change to a more stable site. However, the absence of qualitative changes in the spectra (shift, width, or quadrupolar splittings) with temperature imply that there is no site change in this temperature range, in contrast to Au [7], Ag [8], and Nb [6]. This is somewhat surprising for Bi in particular, where vacancies become mobile around 280 K [109], and the melting temperature is quite low. However, quite high annealing temperatures are required to anneal Li-doped Bi crystals [34].

The distinct quadrupolar splitting in Bi provides a characteristic signature of the site. Calculations and further measurements (rotation patterns and β NQR) are required to precisely identify the site. The situation in the other materials is less clear, but the linewidths provide an estimate of the upper limit of the EFG, also constraining possible sites.

C. $^8Li^+$ shift and relaxation

We now consider the temperature-dependent shifts presented in Fig. 5. First, *the shifts do not scale with the macroscopic susceptibility* χ. This is particularly evident for $Bi_{0.9}Sb_{0.1}$ where χ is largest and most strongly temperature dependent, and the shift K is nearly temperature independent. The lack of correlation with the macroscopic χ is surprising in light of the μSR [89,93], and shows that we are sensitive to hidden aspects of the electronic structure that are not evident in the macroscopic χ. The shift of the insulator $Bi_{0.9}Sb_{0.1}$ is so dramatically different in its temperature dependence that it is natural to seek an explanation of $K(T)$ in the Fermi-surface spin response of the semimetals. A clear measurement of $\chi_{\rm Pauli}$ would constitute an important test of theoretical calculations. Here, we show that a simple quantitative interpretation in Bi is unable to account for the observed $K(T)$, and suggest some other effects that should be included.

We begin with the relaxation. The Korringa law predicts for a metal that $1/T_1$ is linear in T and, moreover, that the Korringa product

$$T_1 T K_{\rm spin}^2 = S, \tag{10}$$

a constant, with a value 1.20×10^{-5} sK for ^{8}Li, where the spin-only Knight shift is

$$K_{\rm spin} = A\chi_{\rm Pauli}. \tag{11}$$

Electron correlations, even in simple metals, often act to slow the Korringa relaxation, making the product somewhat larger. For ^{8}Li, this enhancement is found to be quite small [7], and as we expect correlations to be even weaker in bismuth, we neglect them in using Eq. (10) to estimate $K_{\rm spin}$.

The $1/T_1$ data in Fig. 7 present a number of surprising aspects. First, Sb, with the highest carrier density, has by far the slowest $1/T_1$, and it is not T linear, unlike the zero-field Sb NQR relaxation [87]. In contrast, the semiconducting alloy, with the lowest carrier density, shows the fastest relaxation, and $1/T_1$ exhibits two steplike increases at about 50 and 225 K. The relaxation in bismuth is simplest, behaving linearly as might be expected, however, the value of the slope is about $\frac{2}{3}$ what we find in Au [7], where the carrier density is several orders of magnitude larger. We defer discussion of these unexpected features, and if we simply assume the slope in Bi follows Eq. (10), we estimate $|K_{\rm spin}| \approx 60$ ppm, about 50% of the observed shift at low T [see Fig. 5(b)].

For the simplest model of the temperature-dependent Knight shift in bismuth, we assume

$$K = K_{\rm spin}(T) + K_{\rm orb}, \tag{12}$$

i.e., K is composed of a conventional Knight shift as in Eq. (11) plus a finite offset representing the orbital shift $K_{\rm orb}$. We can make a first approximation for $\chi_{\rm Pauli}(T)$ by taking the usual Fermi integral [78], using the approximately parabolic density of states of Eq. (7), i.e., that will account for thermal carrier excitation. For an ideally parabolic $\rho(\epsilon)$, $\chi_{\rm Pauli}$ can be expressed in terms of the dilogarithm function, but here we simply calculate the integral numerically and allow the parabola to be centered slightly away from the Fermi energy, in agreement with the tight-binding estimate [60]. Here, we also compute the full integral, rather than an expansion in powers of T as in Ref. [78]. As expected, $\chi_{\rm Pauli}$ is an *increasing* function of T, so to be consistent with an increasing $K(T)$, A must be positive with $K_{\rm orb}$ being large and negative. However, the computed $\chi_{\rm Pauli}(T)$ shows a significant upward curvature over this temperature range (see Fig. 10), while $K(T)$ is curved

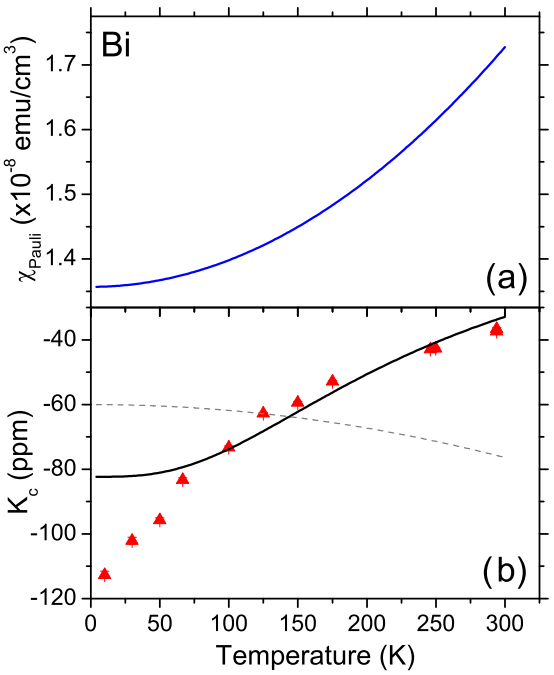

FIG. 10. (Color online) (a) The calculated Pauli susceptibility for bismuth matched to the Sommerfeld estimate at low temperature [21]. (b) A fit (solid curve) of the corrected shift in Bi to Eq. (13) with $K_{\rm spin}(T)$ constrained to -60 ppm (A is negative) at low temperature and to follow the temperature dependence in (a). This $K_{\rm spin}(T)$ is shown as the dashed curve.

downward, so one cannot obtain agreement with this simple form. An obvious generalization is to allow the orbital shift to have a temperature dependence, from the predominant valence band orbital response,

$$K = A\chi_{\rm Pauli}(T) + B\chi_{\rm VB}(T) + C, \tag{13}$$

where B is the orbital hyperfine coupling, and C represents a T-independent orbital contribution from the ion cores. A large orbital shift is consistent with suggestions for Bi NMR [99] and PAD [97,98]. In our view, the muon shift K_μ [89,93] can be accounted for entirely by the B and C terms, with a negligible contribution from A. The T dependence of $\chi_{\rm Pauli}$ in Fig. 10(a) is qualitatively similar to the bulk χ [Fig. 5(c)]: it is increasing with upward curvature, so if the model applies, then A and B cannot have the same sign, assuming $\chi_{\rm VB}(T)$ differs from $\chi(T)$ only by a constant. We can further constrain Eq. (13) using the Korringa law value for $K_{\rm spin}$; however, as χ in Fig. 10 is temperature dependent, it is not clear at which temperature to fix $K_{\rm spin} = \pm 60$ ppm. The relative change with temperature is, however, not very large, so we can still confine $K_{\rm spin}(T = 0)$ within a reasonably narrow range. As shown in Fig. 10(b), the best fit based on this strategy is not adequate to describe the data which are most strongly temperature dependent at low temperature and saturating towards 300 K.

We are thus led to conclude that our model is too crude to capture the essential temperature dependence, and it will be necessary to account for the strongly coupled spin and orbital responses, projected onto the spin degree of freedom by a weak contact hyperfine coupling, and onto the orbital degree of freedom by an orbital coupling dependent, as well, on the $^8Li^+$ site, acting in concert. However, the similarity of $K(T)$ in Sb, with a significantly weaker $\lambda_{\rm SO}$, suggests that an additional consideration, namely, the evolution of the electronic spectrum from the smooth approximately parabolic continuum at high temperature to discrete Landau levels at low temperature [44], might well account for the steeper than expected temperature dependence at low T. If this is the case, we can anticipate quantum oscillations in the NMR shift [110] and relaxation [111] at low T. Clearly, further measurements as a function of field at low temperature are required to test this. Another perturbing effect of the magnetic field, particular to bismuth, due to the multiplicty of the L-point electrons, is revealed by the angle-dependent magnetoresistance at room temperature [112].

We return now to the T dependence of $1/T_1$. The systematics of the relaxation rate with carrier density and temperature are difficult to reconcile if one assumes the standard metallic picture that would have the fastest (and T-linear) relaxation for Sb and the slowest for the semiconductor. Disorder may play an important role, and one may need to consider effects beyond the coherent potential approximation for the alloy. However, as the bulk χ of all three materials, and a substantial fraction of the shift in Bi, is orbital in origin, we should consider the role of *orbital relaxation* [113] caused by current fluctuations due to the orbital motion of free carriers, i.e., the dynamic counterpart of the time-averaged orbital shift.

$(1/T_1)_{\rm orb}$ makes a negligible contribution in conventional NMR in the $A15$ compounds, for example [114], where the core-polarization contact hyperfine coupling dominates, but in some d-band metals, such as vanadium, it appears to be important [75]. Theory suggests long-range orbital current fluctuations may be an effective relaxation mechanism in metals [115,116], and Varma [117] has emphasized its potential role in cuprate NMR as well as in a theory of high-T_c superconductivity [118]. However, none of these calculations take spin-orbit coupling into account. The contact hyperfine coupling for $^8Li^+$ is generally much weaker than for transition-metal NMR, and orbital relaxation may be relatively more important. Indeed, it seems unreasonable that the ^{8}Li hyperfine coupling alone could account for a Korringa slope in Bi comparable to Au. From theory, $(1/T_1)_{\rm orb}$ in a metal is also T linear [113], and if the relaxation in Bi is predominantly orbital, we can at least propose an explanation for the other materials. Specifically, the orbital susceptibility is maximally negative in $Bi_{1-x}Sb_x$ when the Fermi level falls in the gap [see Fig. 5(c)], i.e., for the semiconductor which also shows the largest $1/T_1$. Theory has recently shown, using the Dirac spectrum, and including $\lambda_{\rm SO}$, that a remarkably different quantity, the spin Hall coefficient, follows an *identical* dependence to $\chi_{\rm orb}$ [119]. With its much larger gap, and less Dirac-type spectrum, $(1/T_1)_{\rm orb}$ might well be much smaller in Sb, sufficient to allow other relaxation mechanisms to dominate, leading to the observed nonlinear T dependence. This would also imply a negligible hyperfine coupling in Sb to account for the difference with the NQR $1/T_1$ [87]. One possibility is additional $1/T_1$ due to $^8Li^+$ diffusion at high temperature, consistent with room-temperature electrochemical insertion [120]; however, there is little evidence of the motional narrowing in Fig. 5(d) that one would expect below the onset of diffusional $1/T_1$. Detailed theoretical calculations are required to test this proposal, and such calculations would necessarily include a realistic treatment of thermally excited carriers.

While strong orbital effects may explain the systematics of $1/T_1$, this does not seem to be the case for the shift, where the most diamagnetic $Bi_{0.9}Sb_{0.1}$ with the strongest T dependence in χ has a comparable shift with the least T dependence. This suggests that with $^8Li^+$ in $Bi_{1-x}Sb_x$, we are in the opposite limit to the case of the ^{51}V NMR in the $A15$ superconductors, where orbital effects dominate the shift, but make no contribution to the relaxation [114].

V. CONCLUSIONS

We measured the NMR of $^8Li^+$ implanted at depths on the order of 100 nm into Bi, Sb, and $Bi_{0.9}Sb_{0.1}$. We find negative Knight shifts in all three, with an approximately temperature-independent shift for the insulating phase and qualitatively similar temperature-dependent shifts in the semimetals. A significant fraction of the shift is likely of orbital origin, related to the bulk orbital diamagnetism, but unlike the muon shift, $K(T)$ appears to contain both orbital and spin response, yielding a temperature dependence distinct from the bulk $\chi(T)$, and suggesting it may be possible to extract the spin projection of the response, provided the orbital shift can be calculated. The distinct $K(T)$ compared to the muon shift is likely a result of a larger hyperfine coupling for $^8Li^+$. However, a simple model of $\chi_{\rm Pauli}$ was unable to account for $K(T)$ whose

stronger than expected T dependence at low temperature in both Bi and Sb suggests that Landau quantization may play a role. We find temperature-dependent spin-lattice relaxation, that is linear (metallic) only in Bi, is slowest in the most metallic Sb, and fastest in the insulating alloy, and we suggest that orbital relaxation is predominant in Bi and $Bi_{0.9}Sb_{0.1}$. More experiments and theoretical input are required to test these possibilities.

At the phenomenological level, these initial results indicate a remarkable sensitivity of the implanted $^8Li^+$ to low carrier densities in the semimetals, and qualitatively different behavior in the insulating compound. The prospects for studying the conventional [60] and topological metallic surface states in Bi and $Bi_{0.9}Sb_{0.1}$ are thus good. However, until now, such efforts have been frustrated by backscattering of the probe ion beam at very low energies [121], particularly backscattering accompanied by neutralization [122] that gives rise to a substantial background signal from ^8Li, stopping outside the sample.

ACKNOWLEDGMENTS

We thank D. A. Bonn and B. J. Ramshaw for providing the bismuth crystal, S. Daviel, R. Abasalti, and D. Vyas and the TRIUMF CMMS for technical assistance, G. Levy for crystal alignment, and D. E. MacLaughlin, S. F. J. Cox, and J. H. Brewer for critical reading of the manuscript. We have also benefited from discussions with D. Maslov and K. Behnia, and we thank F. N. Gygax for some unpublished μSR results, and H. Fukuyama for communicating some of his recent results. The crystal growth at Princeton was supported by the Air Force Office of Scientific Research, Grant No. FA9550-10-1-0553, and the measurements by Natural Sciences and Engineering Research Council of Canada.

[1] Z. Salman, O. Ofer, M. Radovic, H. Hao, M. Ben Shalom, K. H. Chow, Y. Dagan, M. D. Hossain, C. D. P. Levy, W. A. MacFarlane, G. M. Morris, L. Patthey, M. R. Pearson, H. Saadaoui, T. Schmitt, D. Wang, and R. F. Kiefl, Phys. Rev. Lett. **109**, 257207 (2012).

[2] Q. Song, K. H. Chow, Z. Salman, H. Saadaoui, M. D. Hossain, R. F. Kiefl, G. D. Morris, C. D. P. Levy, M. R. Pearson, T. J. Parolin, I. Fan, T. A. Keeler, M. Smadella, D. Wang, K. M. Yu, X. Liu, J. K. Furdyna, and W. A. MacFarlane, Phys. Rev. B **84**, 054414 (2011).

[3] Z. Salman, R. F. Kiefl, K. H. Chow, M. D. Hossain, T. A. Keeler, S. R. Kreitzman, C. D. P. Levy, R. I. Miller, T. J. Parolin, M. R. Pearson, H. Saadaoui, J. D. Schultz, M. Smadella, D. Wang, and W. A. MacFarlane, Phys. Rev. Lett. **96**, 147601 (2006).

[4] W. A. MacFarlane, T. J. Parolin, T. I. Larkin, G. Richter, K. H. Chow, M. D. Hossain, R. F. Kiefl, C. D. P. Levy, G. D. Morris, O. Ofer, M. R. Pearson, H. Saadaoui, Q. Song, and D. Wang, Phys. Rev. B **88**, 144424 (2013).

[5] O. Ofer, K. H. Chow, I. Fan, M. Egilmez, T. J. Parolin, M. D. Hossain, J. Jung, Z. Salman, R. F. Kiefl, C. D. P. Levy, G. D. Morris, M. R. Pearson, H. Saadaoui, Q. Song, D. Wang, and W. A. MacFarlane, Phys. Rev. B **86**, 064419 (2012).

[6] T. J. Parolin, J. Shi, Z. Salman, K. H. Chow, P. Dosanjh, H. Saadaoui, Q. Song, M. D. Hossain, R. F. Kiefl, C. D. P. Levy, M. R. Pearson, and W. A. MacFarlane, Phys. Rev. B **80**, 174109 (2009).

[7] T. J. Parolin, Z. Salman, K. H. Chow, Q. Song, J. Valiani, H. Saadaoui, A. O'Halloran, M. D. Hossain, T. A. Keeler, R. F. Kiefl, S. R. Kreitzman, C. D. P. Levy, R. I. Miller, G. D. Morris, M. R. Pearson, M. Smadella, D. Wang, M. Xu, and W. A. MacFarlane, Phys. Rev. B **77**, 214107 (2008).

[8] G. D. Morris, W. A. MacFarlane, K. H. Chow, Z. Salman, D. J. Arseneau, S. Daviel, A. Hatakeyama, S. R. Kreitzman, C. D. P. Levy, R. Poutissou, R. H. Heffner, J. E. Elenewski, L. H. Greene, and R. F. Kiefl, Phys. Rev. Lett. **93**, 157601 (2004).

[9] Y. Ando, J. Phys. Soc. Jpn. **82**, 102001 (2013).

[10] R. J. Cava, H. Ji, M. K. Fuccillo, Q. D. Gibson, and Y. S. Hor, J. Mater. Chem. C **1**, 3176 (2013).

[11] B. Yan and S.-C. Zhang, Rep. Prog. Phys. **75**, 096501 (2012).

[12] M. Z. Hasan and J. E. Moore, Annu. Rev. Condens. Matter **2**, 55 (2011).

[13] D. Hsieh, D. Qian, L. Wray, Y. Xia, Y. S. Hor, R. J. Cava, and M. Z. Hasan, Nature (London) **452**, 970 (2008).

[14] D. Connor, Phys. Rev. Lett. **3**, 429 (1959).

[15] A. Schenck, *Muon Spin Rotation Spectroscopy* (Adam Hilger, London, 1985).

[16] J. H. Brewer, in *Digital Encyclopedia of Applied Physics*, edited by G. L. Trigg (Wiley-VCH, Weinheim, 2003).

[17] H. Ackermann, P. Heitjans, and H.-J. Stöckmann, in *Hyperfine Interactions of Radioactive Nuclei*, Topics in Current Physics, Vol. 31, edited by J. Christiansen (Springer, Berlin, 1983), pp. 291–361.

[18] C. Levy, R. Baartman, K. Jayamanna, R. Kiefl, T. Kuo, M. Olivo, G. Wight, D. Yuan, and A. Zelenski, Nucl. Phys. A **701**, 253 (2002).

[19] G. D. Morris, Hyp. Int. **225**, 173 (2014).

[20] W. A. MacFarlane, T. J. Parolin *et al.*, J. Phys.: Conf. Ser. **551** (to be published).

[21] G. C. Carter, L. H. Bennett, and D. J. Kahan, Prog. Mater. Sci. **20**(Part 1), 1 (1976).

[22] J. F. Ziegler, J. P. Biersack, and U. Littmark, *The Stopping and Range of Ions in Solids* (Pergamon, New York, 1985).

[23] D. S. Gemmell, Rev. Mod. Phys. **46**, 129 (1974).

[24] M. Xu, M. Hossain, H. Saadaoui, T. Parolin, K. Chow, T. Keeler, R. Kiefl, G. Morris, Z. Salman, Q. Song, D. Wang, and W. MacFarlane, J. Magn. Reson. **191**, 47 (2008).

[25] D. Shoenberg and M. Z. Uddin, Proc. R. Soc. London, Ser. A **156**, 687 (1936).

[26] D. Shoenberg and M. Uddin, Math. Proc. Cambridge Philos. Soc. **32**, 499 (1936).

[27] S. H. Browne and C. T. Lane, Phys. Rev. **60**, 899 (1941).

[28] L. Wehrli, Phys. Kondens. Mater. **8**, 87 (1968).

[29] M. H. Cohen and F. Reif, Solid State Phys. **5**, 321 (1957).

[30] W. A. MacFarlane, C. D. P. Levy *et al.*, J. Phys.: Conf. Ser. **551** (to be published).

[31] S. Vega, T. W. Shattuck, and A. Pines, Phys. Rev. Lett. **37**, 43 (1976).

[32] B. Lenoir, M. Cassart, J.-P. Michenaud, H. Scherrer, and S. Scherrer, J. Phys. Chem. Solids **57**, 89 (1996).

[33] L. Fu and C. L. Kane, Phys. Rev. B **76**, 045302 (2007).
[34] C. M. Orovets, A. M. Chamoire, H. Jin, B. Wiendlocha, and J. P. Heremans, J. Electron. Mater. **41**, 1648 (2012).
[35] D. Shoenberg, *Magnetic Oscillations in Metals*, Cambridge Monographs on Physics (Cambridge University Press, Cambridge, UK, 1984).
[36] M. Dresselhaus, J. Phys. Chem. Solids **32** (Suppl. 1), 3 (1971).
[37] V. S. Édel'man, Usp. Fiz. Nauk **123**, 257 (1977) [Sov. Phys.–Usp. **20**, 819 (1977)].
[38] M. H. Cohen, Phys. Rev. **121**, 387 (1961).
[39] X. Gonze, J.-P. Michenaud, and J.-P. Vigneron, Phys. Rev. B **41**, 11827 (1990).
[40] A. B. Shick, J. B. Ketterson, D. L. Novikov, and A. J. Freeman, Phys. Rev. B **60**, 15484 (1999).
[41] Y. M. Koroteev, G. Bihlmayer, E. V. Chulkov, and S. Blügel, Phys. Rev. B **77**, 045428 (2008).
[42] Y. Liu and R. E. Allen, Phys. Rev. B **52**, 1566 (1995).
[43] L. Li, J. G. Checkelsky, Y. S. Hor, C. Uher, A. F. Hebard, R. J. Cava, and N. P. Ong, Science **321**, 547 (2008).
[44] Z. Zhu, B. Fauqué, Y. Fuseya, and K. Behnia, Phys. Rev. B **84**, 115137 (2011).
[45] P. Wolff, J. Phys. Chem. Solids **25**, 1057 (1964).
[46] H. Fukuyama, Y. Fuseya, M. Ogata, A. Kobayashi, and Y. Suzumura, Phys. B (Amsterdam) **407**, 1943 (2012).
[47] Y. Fuseya, M. Ogata, and H. Fukuyama, J. Phys. Soc. Jpn. (to be published).
[48] P. J. Lin and L. M. Falicov, Phys. Rev. **142**, 441 (1966).
[49] G. Harte, M. Priestley, and J. Vuillemin, J. Low Temp. Phys. **31**, 897 (1978).
[50] L. S. Lerner, K. F. Cuff, and L. R. Williams, Rev. Mod. Phys. **40**, 770 (1968).
[51] P. Cucka and C. S. Barrett, Acta Crystallogr. **15**, 865 (1962).
[52] J. C. Y. Teo, L. Fu, and C. L. Kane, Phys. Rev. B **78**, 045426 (2008).
[53] B. Lenoir, M. O. Selme, A. Demouge, H. Scherrer, Y. V. Ivanov, and Y. I. Ravich, Phys. Rev. B **57**, 11242 (1998).
[54] N. Harrison and S. E. Sebastian, New J. Phys. **14**, 095023 (2012).
[55] D. Singh, Phys. C (Amsterdam) **469**, 418 (2009).
[56] E. Gerlach, P. Grosse, M. Rautenberg, and W. Senske, Phys. Status Solidi B **75**, 553 (1976).
[57] R. Tediosi, N. P. Armitage, E. Giannini, and D. van der Marel, Phys. Rev. Lett. **99**, 016406 (2007).
[58] X. Du, S.-W. Tsai, D. L. Maslov, and A. F. Hebard, Phys. Rev. Lett. **94**, 166601 (2005).
[59] Y. Kopelevich, J. C. Medina Pantoja, R. R. da Silva, and S. Moehlecke, Phys. Rev. B **73**, 165128 (2006).
[60] P. Hofmann, Prog. Surf. Sci. **81**, 191 (2006).
[61] N. Garcia, Y. H. Kao, and M. Strongin, Phys. Rev. B **5**, 2029 (1972).
[62] T. W. Cornelius, M. E. Toimil-Molares, S. Karim, and R. Neumann, Phys. Rev. B **77**, 125425 (2008).
[63] A. M. Clogston, V. Jaccarino, and Y. Yafet, Phys. Rev. **134**, A650 (1964).
[64] F. A. Buot and J. W. McClure, Phys. Rev. B **6**, 4525 (1972).
[65] M. H. Cohen and E. I. Blount, Philos. Mag. **5**, 115 (1960).
[66] G. E. Smith, G. A. Baraff, and J. M. Rowell, Phys. Rev. **135**, A1118 (1964).
[67] H. Fukuyama and R. Kubo, J. Phys. Soc. Jpn. **28**, 570 (1970).
[68] H. Fukuyama, Prog. Theor. Phys. **45**, 704 (1971).
[69] E. N. Adams, Phys. Rev. **89**, 633 (1953).
[70] N. Brandt, M. Semenov, and L. Falkovsky, J. Low Temp. Phys. **27**, 75 (1977).
[71] M. P. Vecchi and M. S. Dresselhaus, Phys. Rev. B **10**, 771 (1974).
[72] F. A. Buot, J. Phys. Chem. Solids **32** (Suppl. 1), 99 (1971).
[73] T. Thonhauser, Int. J. Mod. Phys. B **25**, 1429 (2011).
[74] J. van der Klink and H. Brom, Prog. NMR Spectrosc. **36**, 89 (2000).
[75] R. E. Walstedt, in *The NMR Probe of High-Tc Materials*, Springer Tracts in Modern Physics, Vol. 228 (Springer, Berlin, 2008), pp. 13–65.
[76] N. Bloembergen, Physica (Amsterdam) **20**, 1130 (1954).
[77] D. Wolf, *Spin-Temperature and Nuclear-Spin Relaxation in Matter*, International Series of Monographs on Physics (Oxford University Press, Oxford, UK, 1979).
[78] M. J. R. Hoch and D. F. Holcomb, Phys. Rev. B **71**, 035115 (2005).
[79] C. S. Lue and J. H. Ross, Phys. Rev. B **63**, 054420 (2001).
[80] J. Y. Leloup, B. Sapoval, and G. Martinez, Phys. Rev. B **7**, 5276 (1973).
[81] S. D. Senturia, A. C. Smith, C. R. Hewes, J. A. Hofmann, and P. L. Sagalyn, Phys. Rev. B **1**, 4045 (1970).
[82] R. L. Hota, R. C. Patnaik, G. S. Tripathi, and P. K. Misra, Phys. Rev. B **51**, 7291 (1995).
[83] R. E. Taylor, F. Alkan, D. Koumoulis, M. P. Lake, D. King, C. Dybowski, and L.-S. Bouchard, J. Phys. Chem. C **117**, 8959 (2013).
[84] B. F. Williams and R. R. Hewitt, Phys. Rev. **146**, 286 (1966).
[85] A. D. Goldsmith and R. R. Hewitt, Phys. Rev. B **12**, 4640 (1975).
[86] R. R. Hewitt and D. E. MacLaughlin, J. Magn. Reson. **30**, 483 (1978).
[87] G. Hill, J. Keartland, and M. Hoch, Phys. B (Amsterdam) **279**, 319 (2000).
[88] F. N. Gygax, A. Schenck, A. J. van der Wal, and S. Barth, Phys. Rev. Lett. **56**, 2842 (1986).
[89] S. Barth, P. Birrer, F. Gygax, B. Hitti, E. Lippelt, and A. Schenck, Hyp. Int. **51**, 881 (1989).
[90] O. Hartmann, E. Karlsson, L.-O. Norlin, K. Pernestål, M. Borghini, and T. Niinikoski, Hyp. Int. **4**, 828 (1978).
[91] J. Brewer, D. Harshman, E. Koster, H. Schilling, D. Williams, and M. Priestley, Solid State Commun. **46**, 863 (1983).
[92] T. Johnston, K. Chow, S. Dunsiger, T. Duty, R. Kiefl, E. Koster, W. MacFarlane, G. Morris, J. Sonier, and D. Williams, Hyp. Int. **106**, 71 (1997).
[93] E. Lippelt, P. Birrer, F. Gygax, B. Hitti, A. Schenck, and M. Weber, Z. Phys. B **86**, 367 (1992).
[94] S. F. J. Cox, Rep. Prog. Phys. **72**, 116501 (2009).
[95] S. J. Blundell and S. F. J. Cox, J. Phys.: Condens. Matter **13**, 2163 (2001).
[96] J. A. Chakhalian, R. F. Kiefl, S. R. Dunsiger, W. A. MacFarlane, R. Miller, J. E. Sonier, and J. E. Fischer, Phys. Rev. B **66**, 155107 (2002).
[97] A. Berger, H. Bertschat, H.-E. Mahnke, B. Spellmeyer, and W. Shen, Hyp. Int. **34**, 547 (1987).
[98] W. Shen, A. Berger, H. Bertschat, H.-E. Mahnke, and B. Spellmeyer, Phys. Lett. A **125**, 489 (1987).
[99] R. E. Watson, L. H. Bennett, G. C. Carter, and I. D. Weisman, Phys. Rev. B **3**, 222 (1971).

[100] P. Heitjans, G. Kiese, C. van Der Marel, H. Ackermann, B. Bader, P. Freiländer, and H.-J. Stöckmann, Hyp. Int. **16**, 569 (1983).
[101] T. P. Das and E. H. Sondheimer, Philos. Mag. **5**, 529 (1960).
[102] Y. Yafet, J. Phys. Chem. Solids **21**, 99 (1961).
[103] J. E. Hebborn and M. J. Stephen, Proc. Phys. Soc. **80**, 991 (1962).
[104] C. Frétigny, M. Saint Jean, and M.-F. Quinton, Phys. Rev. B **49**, 9586 (1994).
[105] F. Mauri, B. G. Pfrommer, and S. G. Louie, Phys. Rev. Lett. **77**, 5300 (1996).
[106] M. d'Avezac, N. Marzari, and F. Mauri, Phys. Rev. B **76**, 165122 (2007).
[107] T. Thonhauser, D. Ceresoli, A. A. Mostofi, N. Marzari, R. Resta, and D. Vanderbilt, J. Chem. Phys. **131**, 101101 (2009).
[108] G. Solt, E. Lippelt, and B. Delley, Phys. Rev. B **44**, 4843 (1991).
[109] S. Otake, Y. Ishii, and N. Matsuno, Jpn. J. Appl. Phys. **20**, 1037 (1981).
[110] R. G. Goodrich, S. A. Khan, and J. M. Reynolds, Phys. Rev. B **3**, 2379 (1971).
[111] F. Bridges and W. G. Clark, Phys. Rev. **182**, 463 (1969).
[112] Z. Zhu, A. Collaudin, B. Fauqué, W. Kang, and K. Behnia, Nat. Phys. **8**, 89 (2012).
[113] Y. Obata, J. Phys. Soc. Jpn. **18**, 1020 (1963).
[114] A. M. Clogston, A. C. Gossard, V. Jaccarino, and Y. Yafet, Phys. Rev. Lett. **9**, 262 (1962).
[115] P. Lee and N. Nagaosa, Phys. Rev. B **43**, 1223 (1991).
[116] A. Knigavko, B. Mitrović, and K. V. Samokhin, Phys. Rev. B **75**, 134506 (2007).
[117] C. M. Varma, Phys. Rev. Lett. **77**, 3431 (1996).
[118] C. M. Varma, Phys. Rev. Lett. **83**, 3538 (1999).
[119] Y. Fuseya, M. Ogata, and H. Fukuyama, J. Phys. Soc. Jpn. **83**, 074702 (2014).
[120] A. Darwiche, C. Marino, M. T. Sougrati, B. Fraisse, L. Stievano, and L. Monconduit, J. Am. Chem. Soc. **134**, 20805 (2012).
[121] H. Brongersma, M. Draxler, M. de Ridder, and P. Bauer, Surf. Sci. Rep. **62**, 63 (2007).
[122] J. Los and J. Geerlings, Phys. Rep. **190**, 133 (1990).